

Article

Cost-Effective Preparation of Gold Tailing-Based Aerogels for Efficient Adsorption of Copper Ions from Wastewater

Yingjie Wang ¹, Kaibin Cui ², Jiaxuan Bai ², Baizeng Fang ^{3,*}  and Fei Wang ^{2,*}¹ Hebei Ruisuo Solid Waste Engineering Technology Research Institute Co., Ltd., Chengde 067020, China² Key Laboratory of Special Functional Materials for Ecological Environment and Information, Hebei University of Technology, Ministry of Education, Tianjin 300130, China³ Department of Energy Storage Science and Technology, University of Science and Technology Beijing, 30 College Road, Beijing 100083, China

* Correspondence: baizengfang@163.com (B.F.); wangfei@hebut.edu.cn (F.W.)

Abstract: Water pollution caused by heavy metal ions has attracted worldwide attention. In this work, gold tailings were used as raw materials and the sol–gel method combined with the atmospheric pressure drying method were used to achieve the low-cost preparation of a silica aerogel. (3-Aminopropyl) triethoxysilane (APTES), ethylenediaminetetraacetic acid disodium salt (EDTA-2Na), and chitosan were used to modify the silica aerogel, which was then used as an adsorbent for the adsorption of copper ions in wastewater. The adsorbent type, adsorption time, copper ion concentration, and pH value were investigated as variables to explore the best adsorption conditions. The adsorption mechanism was also elaborated on. The crystal structure, surface morphology, surface functional groups, chemical composition, and specific surface area of the aerogels and the modified aerogels were characterized by various physiochemical characterizations such as XRD, SEM, FT-IR, XRF, and BET. The results showed that the prepared silica aerogel contained 91.1% SiO₂, mainly amorphous SiO₂, and amino and carboxyl groups. Other functional groups were successfully grafted onto the silica aerogels. The original silica aerogels and modified silica aerogels had a large specific surface area, total pore volume, and pore diameter. When copper ions were adsorbed by the chitosan-modified silica aerogels, the adsorption capacity of the copper ions was the highest (33.51 mg/g) under the conditions of a copper ion concentration of 100 mg/L, a pH value of 7, and an adsorption time of 2 h. The adsorption of Cu²⁺ was mainly due to the ion exchange and electrostatic gravity.

Keywords: gold tailings; silica aerogel; copper ions; adsorption; wastewater

check for updates

Citation: Wang, Y.; Cui, K.; Bai, J.; Fang, B.; Wang, F. Cost-Effective Preparation of Gold Tailing-Based Aerogels for Efficient Adsorption of Copper Ions from Wastewater. *Water* **2023**, *15*, 669. <https://doi.org/10.3390/w15040669>

Academic Editors: Silvia Santos, Antonio Turco and Ariana Pintor

Received: 13 December 2022

Revised: 25 January 2023

Accepted: 2 February 2023

Published: 8 February 2023



Copyright: © 2023 by the authors. Licensee MDPI, Basel, Switzerland. This article is an open access article distributed under the terms and conditions of the Creative Commons Attribution (CC BY) license (<https://creativecommons.org/licenses/by/4.0/>).

1. Introduction

Seriously increasing the water pollution of the world has brought enormous harm to human beings and has become one of the most urgent problems in the world [1]. With the rapid development of industrialization, a large number of heavy metal ions have been discharged into the water without treatment, which has aggravated the problem of water pollution. Heavy metal ions such as copper ions have been used in the metallurgical and electronics industries and have played an important role, mainly in printed circuit board etching, electroplating, and other processes. In addition to the important function in modern industry, excessive concentrations of heavy metal ions are toxic and bioaccumulated. If the copper ions in the human body exceed the normal range, copper poisoning will occur, causing jaundice, liver necrosis, gastric ulcers, etc.; this has aroused great social concern [2]. Therefore, removing excess copper ions in wastewater has become an urgent task.

At present, the methods of treating copper ions in common wastewater mainly include the chemical precipitation method [3], ion exchange method [4], membrane separation method [5], ferrite method [6], and adsorption method [7,8]. Among these technologies for the removal of copper ions, adsorption can be regarded as a very promising approach for wastewater purification due to its cost-effectiveness and ease of implementation [9].

The removal of copper ions in water by specific adsorbents, whether from a scientific or practical application point of view, is of great significance to invest in the design and synthesis of cost-effective, stable, and efficient materials to remove copper ions [10].

Nanosilica [11,12], activated carbon [13], aerogels [14], and nano-oxides [15] are often used as adsorbents. Silica aerogel (SA) is a new sponge-like, extremely light solid with an open-cell structure that has attracted great interest among scientists and engineers [16]. Due to their high specific surface area, large average pore size, slow heat transfer, and sparse structure, aerogels, as one of the lightest thermal insulation materials, play a key role in various fields [17]. Under the condition of keeping the three-dimensional skeleton of the colloidal gel unchanged, silica gel was synthesized by replacing the water in the pores of the colloidal gel with air [18]. The structure was relatively sparse, the specific surface area was satisfactory, and the thermal energy barrier effect was good; it has been widely used in heat preservation, sound insulation, catalysis, insulators, etc. [18,19]. As a porous material, its large pores (5–30 nm) make the internal surface of the material more accessible to the target species, leading to rapid chemical or physical kinetic processes. In addition, its thick pore walls provide a strong mechanical stability, which provides a good structure as an adsorbent. SAs have also been widely reported as adsorbents for separating different types of contaminants. For example, the separation effect of silica gel on dyes such as methylene blue and Congo red [20,21] and the separation effect of polluted oil and multichain alcohols in water [22,23] showed considerable adsorption performances [23–25]. Modified aerogels have also shown a good adsorption performance against heavy metal ions such as Cu^{2+} , Pb^{2+} , and Ni^{2+} [26,27]. Pure silicon sources such as sodium silicate and ethyl orthosilicate have been directly used as silica aerogels with a high cost, limiting their application in life. Therefore, finding a low-cost silicon source as a raw material to reduce production costs has become an important task at present.

Gold tailings are a solid by-product of the beneficiation process; China produces billions of tons of gold tailings every year [28]. The storage of gold tailings occupies a lot of land resources and has a great impact on the surrounding environment [29]. The harmful substances in gold tailings can cause serious harm to the natural environment and pose a threat to various aspects such as the social economy and human health. When a large amount of gold tailings is stored in the open air, collapse accidents often occur due to external environmental factors, which have huge safety hazards due to the large accumulation volume and instability. In addition, the exposure of gold tailings to the air produces a large amount of dust, causing acid mine wastewater to pollute the soil and water, resulting in environmental pollution and posing certain hazards to human health. As gold tailings contain relatively rich Si, Al, and Ca oxides, it has a high competitiveness in the manufacture of building materials such as concrete and slurry as well as industrial materials such as glass and ceramics. Due to the high silica content in gold tailings and easy reaction with alkali, gold tailings are a promising silica aerogel raw material [30].

In this work, SA was prepared by the atmospheric pressure drying method combined with a sol–gel method using gold tailings as the raw material, which realized the low-cost preparation of a silica aerogel. APTES, EDTA-2Na, and chitosan were used to modify the silica aerogel. The samples were characterized and analyzed, and the optimal adsorption conditions for copper ions were explored. The adsorption mechanism was also elaborated on, which we believe has an important value in scientific research and environmental protection.

2. Experimental Section

2.1. Materials

(3-Aminopropyl) triethoxysilane (APTES, 99%), EDTA disodium salt solution (EDTA-2Na, 0.2 M), chitosan (deacetylation > 95%, viscosity 100–200 mPa.s), $\text{NH}_3\text{-NH}_4\text{Cl}$ buffer solution (pH 8–10), and sodium diethyldithiocarbamate (DDTC, 98%) were purchased from the Shanghai Macklin Biochemical Co., Ltd. (Shanghai, China). Propanol, glacial acetic

acid (AR), absolute ethanol (AR), hydrochloric acid, and sodium hydroxide (NaOH, AR) were provided by the Tianjin Damao Chemical Reagent Group Co., Ltd. (Tianjin, China).

2.2. Experiment

2.2.1. Synthesis of the Silica Aerogel

First, 10 g of gold tailings were thoroughly mixed with 7.7 g of sodium hydroxide after being screened using a sieve of 0.075 mm and the mixture was calcined at 550 °C for 3 h. After the calcined product was naturally cooled to room temperature, it was added to deionized water and stirred for 2 h and centrifuged; the supernatant was retained. The pH of the supernatant was adjusted to 10 by dilute hydrochloric acid, then the gel reaction was carried out. After the gel was aged for 12 h, it was added to absolute ethanol to further age for 48 h to achieve the solvent replacement. The displacement suspension was filtered and dried at 80 °C for 12 h to obtain the SA.

2.2.2. Synthesis of Amino-Modified SA

After 0.7 g of the SA sample was dispersed in 190 mL of propanol and heated to 80 °C and stirred homogeneously, 1.25 mL of APTES was added dropwise and the mixture was refluxed and stirred at 80 °C for 4 h. Finally, the samples were centrifuged and washed three times with ethanol and dried overnight at 60 °C to obtain the amino-modified aerogels (SA-NH₂).

2.2.3. Synthesis of Carboxyl-Modified SA

The work of grafting the carboxyl was implemented according to previous research [31], and the reaction principle is shown in Figure 1. First, 0.5 g of amino-modified SA was dispersed in 80 mL of EDTA-2Na in water (0.1 M) and stirred for 24 h at room temperature. The samples were then centrifuged, rinsed with distilled water, and dried overnight at 60 °C to obtain the EDTA-2Na-modified SA (SA-COOH).

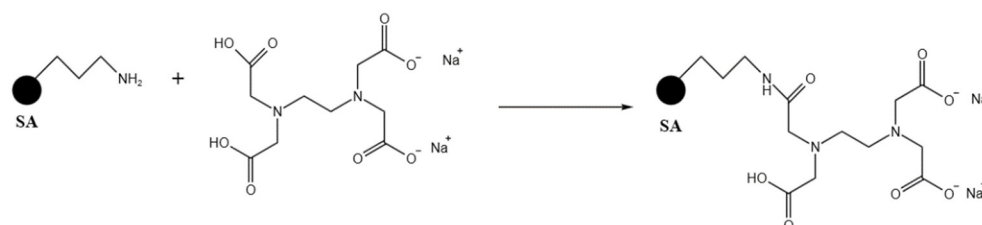


Figure 1. Schematic reaction of SA-NH₂ with EDTA-2Na.

2.2.4. Synthesis of Chitosan-Modified SA

First, 0.3 g of chitosan was dispersed in 40 mL of (2%) acetic acid. After a uniform dispersion, 1 g of SA was added to the above solution and stirred for 1 h. The pH of the above suspension was then adjusted to 6–7 with 0.2 M NaOH. The sample was then centrifuged and washed to neutral with deionized water and ethanol. Finally, it was dried overnight at 60 °C to obtain the chitosan-modified SA (SA-Ch).

2.3. Heavy Metal Adsorption Experiments

In order to test the adsorption capacity of the prepared modified SAs on copper ions at 25 °C, 0.05 g of the different types of modified SAs was added to 50 mL of the copper ion solutions with different concentrations and different pH values; these were stirred for different lengths of time. The frequency of the stirring was 200 r/min. The pH value of the copper ion solution was adjusted with 0.2 M hydrochloric acid or 0.2 M sodium hydroxide and then measured with precision pH test strips. After the adsorption was completed, 5 mL of the supernatant was taken and centrifuged. The equilibrium concentration of the copper ions was determined by the DDTC-Na method [32]; the specific operation was as follows. First, 5 mL of the centrifuged supernatant was added to a cuvette tube, then 10 mL

of the DDTc solution and 10 mL of the $\text{NH}_3\text{-NH}_4\text{Cl}$ buffer were sequentially added to the tube. After mixing evenly, the absorbance was measured at the wavelength of 452 nm with a UV-visible spectrophotometer. The remaining Cu^{2+} concentration in the solution was obtained according to the measured absorbance. Each group of trials was performed five times and the average concentration was calculated. The equilibrium adsorption capacity of the copper ions was calculated according to the following formula:

$$Q_e = \frac{(C_0 - C_e)V}{W} \quad (1)$$

where Q_e (mg/g) was the equilibrium adsorption concentration of the copper ions, C_0 (mg/L) was the initial concentration of the copper ions, C_e (mg/L) was the equilibrium concentration of the copper ions, V (mL) was the volume of the copper ion solution, and W (g) was the mass of the modified SA.

2.4. Characterizations

The crystal structure of the samples was examined by X-ray diffraction (XRD) (Smart-Lab, Tokyo, Japan) using $\text{Cu K}\alpha$ radiation ($\lambda = 0.1541$ nm) at 40 kV and 40 mA. The microscopic morphology of the samples was observed by scanning electron microscopy (SEM) (Nano SEM450, FEI Co., Ltd, Hillsboro, OR, USA) after spraying the gold. The functional groups of the samples were characterized using a Fourier-transform infrared (FT-IR) spectrophotometer (Bruker-TENSOR II) (Bruker Co., Ltd, Billerica, MA, USA) at a scanning range between 4000 and 400 cm^{-1} . The adsorption–desorption isotherm and specific surface area of the samples were measured by a Quantachrome autosorb-iQ₂ analyzer (autosorb IQ₂, Quantachrome, Boynton Beach, FL, USA). The microchemical composition and content of the samples were examined by X-ray fluorescence (XRF) (Rigaku, ZSX Primus II, Osaka, Japan). The particle size distribution was measured by a laser particle size meter (SURPASS3, Anton Paar GmbH, Graz, Austria).

3. Results and Discussion

3.1. Physicochemical Characterizations

Figure 2 shows the XRD patterns of the original SAs and modified SAs. It could be seen that there was no sharp diffraction peak observed for all SA samples, only a wide peak between $20\text{--}30^\circ$, which is a typical characteristic peak of amorphous silica, proving the amorphous structure of the SAs [33–35]. It was found that the intensity of the diffraction peak of the modified SAs decreased to a certain extent, which was probably caused by the coating of the modifiers on their surface.

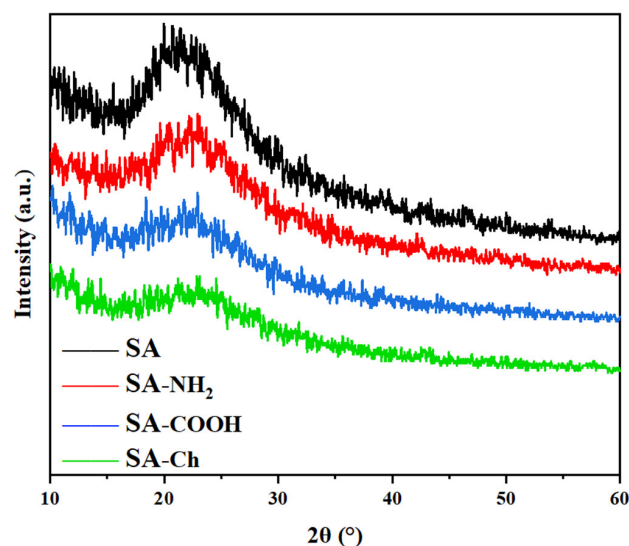


Figure 2. XRD patterns of the original and modified SAs.

Figure 3 shows the FT-IR patterns of the original SA, EDTA-2Na aerogel (SA-COOH), APTES aerogel (SA-NH₂), and chitosan aerogel (SA-Ch). It could be seen that the band around 3440 cm⁻¹ formed characteristic peaks, which were attributed to the telescopic vibration of -OH. The peaks around 1083 cm⁻¹, 795 cm⁻¹, and 472 cm⁻¹ were the asymmetric telescopic, symmetrical, and bending vibrations of the Si-O-Si bonds, respectively [36], typical peaks of SAs [35,37,38]. In the atlas of the modified SAs, it could be seen that the peaks around 2955 cm⁻¹ and 2925 cm⁻¹ were attributed to the symmetrical and asymmetric telescopic vibrations of the -CH₃ bonds and -CH₂- bonds, respectively [39]. The characteristic peaks around 1560 cm⁻¹ were attributed to the bending vibrations of the N-H bonds, indicating that the amino group was successfully grafted onto the surface of the SAs. The strong peak around 1730 cm⁻¹ could be attributed to the contraction vibration of the C=O bonds [40]. The characteristic peak around 1660 cm⁻¹ could be attributed to the contraction vibration of the C=O bonds of the amide group, which is the main band of the amide ligand, indicating that the carboxyl group was successfully grafted onto the surface of the SA [41]. The characteristic peaks around 1328 cm⁻¹ and 3430 cm⁻¹ were attributed to the bending vibration and telescopic vibration of the N-H bonds in chitosan, respectively, indicating that chitosan was successfully grafted onto the surface of the SA.

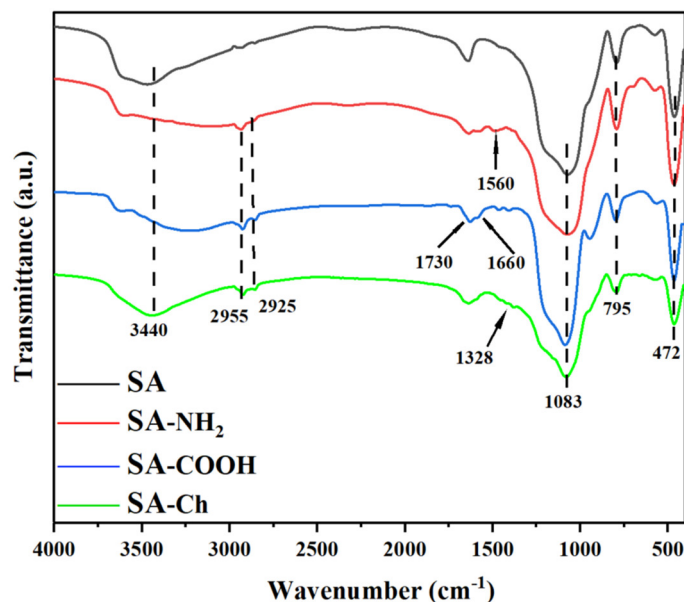


Figure 3. FT-IR patterns of the original and modified SAs.

Figure 4 displays the SEM images of the original SA and the SAs modified by EDTA-2Na, APTES, and chitosan. Figure 5 shows the particle diameter distribution of the original SA and the SAs modified by EDTA-2Na, APTES, and chitosan. It could be seen that the original SA was irregularly spherical and had a relatively good dispersion [42,43] whereas the amino-modified SA had a large area of aggregation. This may have been due to the formation of a new silica propylamine part on the surface of the SA, leading to a decrease in the dispersion and, in turn, the emergence of aggregation. The primary amine produced by the grafted amino group is conducive to the grafting of macromolecular chain groups such as EDTA anhydride on silica [44]; thus, the agglomeration phenomenon after the EDTA-2Na modification was more obvious, indicating that it adhered to the surface of the aerogels. The SAs modified by chitosan also showed aggregation, which was attributed to the coating adhesion of the chitosan macromolecules to the SAs. From Figure 5 and Table 1, it could be seen that the particle size of the original aerogel was smaller than that of the modified aerogel, which may have been caused by particle agglomeration and functional cluster grafting on the SA surface.

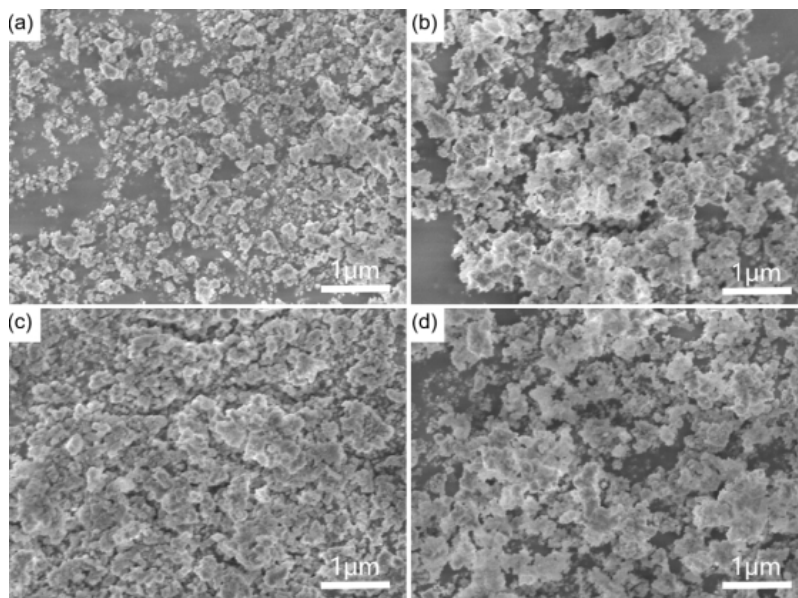


Figure 4. SEM images of SA (a), SA-NH₂ (b), SA-COOH (c), and SA-Ch (d).

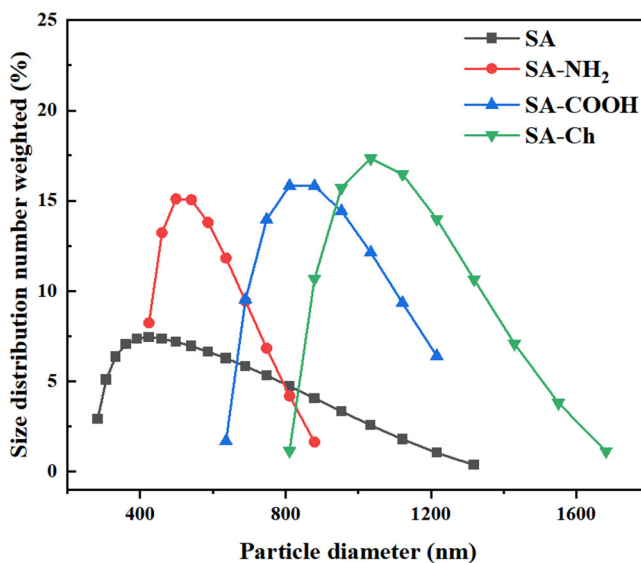


Figure 5. Particle diameter distribution of the original and modified SAs.

Table 1. Average particle diameter of SA, SA-NH₂, SA-COOH, and SA-Ch.

| Sample | SA | SA-NH ₂ | SA-COOH | SA-Ch |
|--------------------------------|-----|--------------------|---------|-------|
| Average particle diameter (nm) | 576 | 667 | 918 | 1195 |

Figure 6 shows the adsorption–desorption isotherm and pore-size distribution of the SA samples. According to the classification of IUPAC, the samples revealed an IV adsorption isotherm; this increases sharply at larger levels of P/P₀ and the formation of hysteresis loops can also be observed [43,45,46]. These isotherms resemble H2-type hysteresis loops, which are characteristic of complex networks of major mesopores that may have bottleneck-type pores. Table 2 shows the textural parameters such as the specific surface area, average pore diameter, and total pore volume for the different SA samples. It could be seen that all samples had a large specific surface area and an average pore diameter and total pore volume, indicating that they had a good adsorbent structure. The modified

SAs had a lower specific surface area than the original SA, which may have been caused by a large number of functional groups grafted onto the SA. The average pore diameter and total pore volume of the modified SAs were also smaller than those of the original SA, which confirmed that the functional groups such as amino groups and carboxyl groups were also grafted onto the internal pores of the SAs.

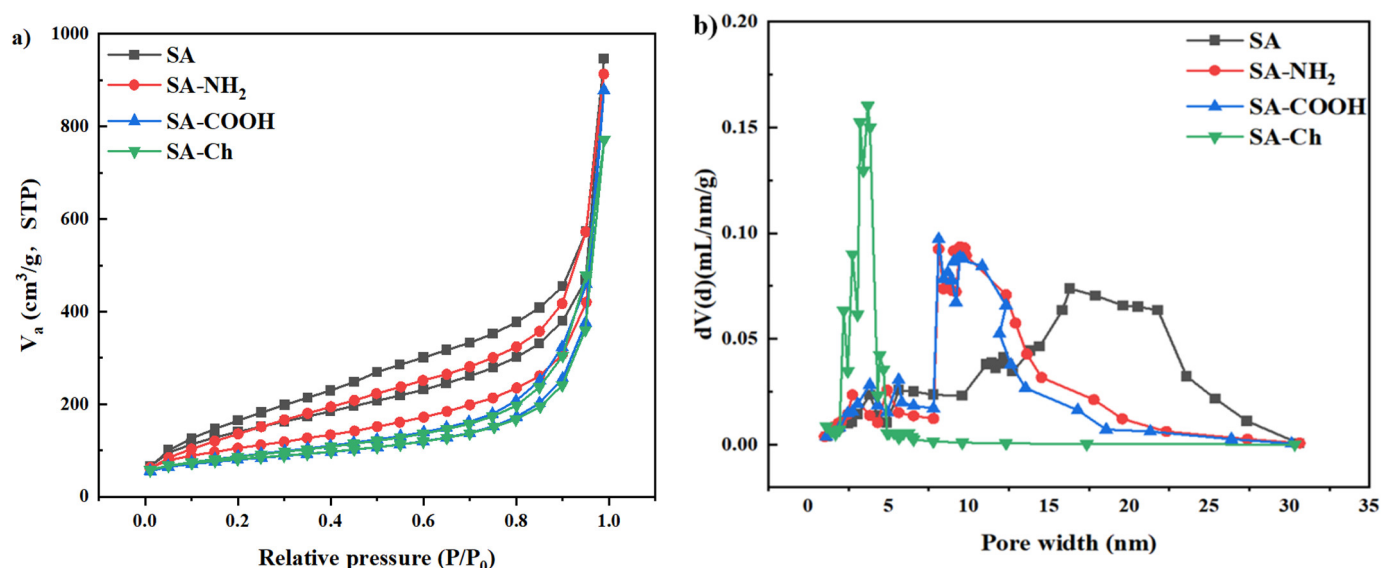


Figure 6. Adsorption–desorption isotherm curves (a) and pore-size distribution (b) of the original SA and modified SAs.

Table 2. Textural parameter summary of SA, SA-NH₂, SA-COOH, and SA-Ch.

| Sample | Specific Surface Area (m^2/g) | Average Pore Diameter (nm) | Total Pore Volume (cc/g) |
|--------------------|---|----------------------------|--|
| SA | 526.245 | 16.245 | 1.514 |
| SA-NH ₂ | 431.256 | 9.822 | 1.403 |
| SA-COOH | 400.421 | 9.523 | 1.366 |
| SA-Ch | 154.662 | 3.563 | 1.064 |

Table 3 summarizes the XRF analysis results of the tailings, alkali melt filter residue, and SA. The data showed that the mass fraction of silica in the prepared SA sample was 91.1%, which was consistent with the results of XRD, indicating that the main component of the SA was silica. The mass fraction of SiO₂ in the tailings was 57.7% before the alkali melting and 41.5% in the remaining filter residue after the alkali melting extraction; thus, the utilization rate of the silicon element was ca. 28%.

Table 3. Main components of the gold tailings, alkali slag, and SA (wt.%).

| | SiO ₂ | Al ₂ O ₃ | Fe ₂ O ₃ | CaO | MgO | K ₂ O | Na ₂ O | TiO ₂ | P ₂ O ₅ | SO ₃ |
|---------------|------------------|--------------------------------|--------------------------------|-------|-------|------------------|-------------------|------------------|-------------------------------|-----------------|
| Gold tailings | 57.7 | 17.2 | 6.33 | 5.97 | 3.77 | 3.74 | 3.02 | 0.627 | 0.317 | 0.683 |
| Alkali slag | 41.5 | 15.0 | 6.63 | 5.73 | 2.54 | 2.03 | 25.1 | 0.605 | 0.128 | 0.206 |
| SA | 91.1 | 3.13 | 0.505 | 0.291 | 0.148 | 0.223 | 3.25 | 0.188 | 0.448 | 0.226 |

3.2. Adsorption Analysis

As DDTC and Cu²⁺ undergo a color reaction in an alkaline environment [32], the principle of a color reaction between DDTC and Cu²⁺ is shown in Figure 7. It could be seen that the molar ratio of Cu²⁺ to DDTC in the chromogenic reaction was 1:2, so an excess DDTC solution was generally used to measure the remaining Cu²⁺ concentration.

The $\text{NH}_3\text{-NH}_4\text{Cl}$ buffer solution was used to ensure the stability of the reaction system at a pH of 8~10. The formation of yellow stable substances and the uniform and stable presence in the reaction system could be directly detected by spectrophotometry at the wavelength of $\lambda = 452 \text{ nm}$. The effective detection range was $0.011\sim 0.071 \text{ mmol L}^{-1}$, which was in accordance with the Lambert–Beer law. Figure 8 shows the absorbance standard fitting curve measured by 0–0.6 mmol/L copper ions under monochromatic illumination at the wavelength of $\lambda = 452 \text{ nm}$. The relationship between the absorbance (y) and copper ion concentration (x) in this range was calculated by curve fitting as $y = 11.11x + 0.0018$ ($R^2 = 0.9993$), so that the copper ion content in water could be calculated according to the measured absorbance.

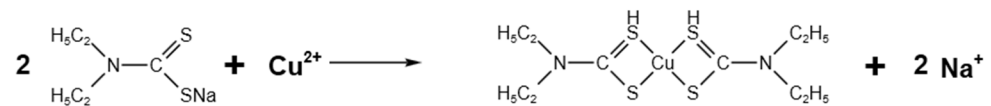


Figure 7. Principle of color reaction between DDTC and Cu^{2+} .

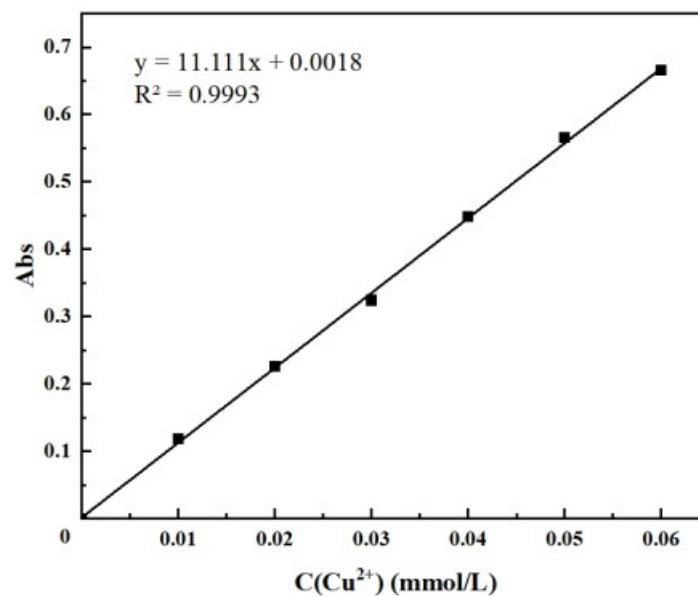
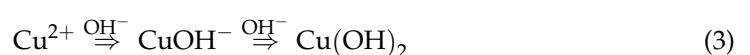
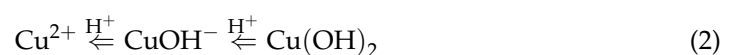


Figure 8. Absorbance standard fitting curve for Cu^{2+} .

To clarify the behavior of the copper ions in the solution and to facilitate the subsequent experimental design, the MEDUSA program was used to determine the presence of copper ions at the tested pH range. Figure 9 shows the presence of copper ions at a concentration of 4 mM (approximately 250 mg/L) at different pH values. It could be clearly seen that when the pH value was smaller than 5.7, the existence form of the copper ions was mainly Cu^{2+} and there was a small amount of CuOH^- ; the content of CuOH^- gradually increased as the pH value increased. When the pH value was greater than 5.7, the content of Cu^{2+} and CuOH^- in the solution began to decrease and Cu(OH)_2 precipitation occurred. When the pH value reached 6, the amount of precipitation reached the maximum. When the pH value reached 8.8, Cu^{2+} could not exist in the solution and was basically converted into a Cu(OH)_2 precipitate. This showed that the copper ions mainly existed in the form of Cu^{2+} in the acidic environments (Equation (2)) and Cu(OH)_2 in the alkaline environments (Equation (3)), which could be expressed as:



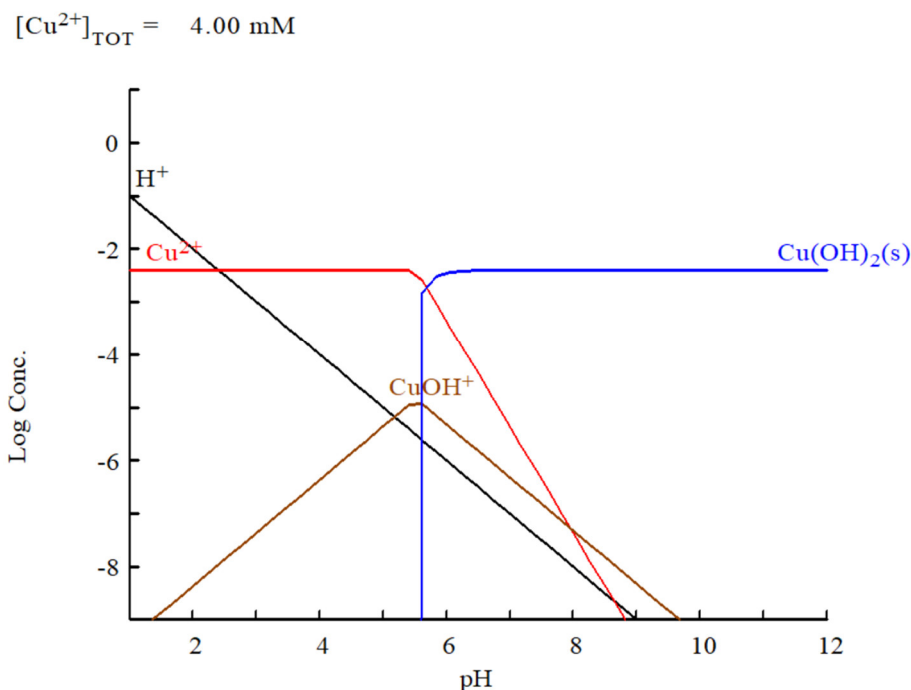


Figure 9. Morphological curve of 4 mM copper ions at different pH values.

In order to study the adsorption capacity of different types of adsorbents, gold tailings, SA, SA-NH₂, SA-COOH, and SA-Ch were added to the solution with a copper ion concentration of 100 mg/L. The pH of the solution was adjusted to 7 and the adsorption was 2 h at room temperature. It is evident from Figure 10 that SA-Ch had the best adsorption performance; its maximum adsorption capacity for Cu²⁺ was 33.51 mg/g. The good adsorption performance of SA-Ch was mainly attributed to the grafting of a large amount of chitosan onto its surface, which was related to the rich hydroxyl groups and amino groups on the surface of chitosan [26], providing abundant attachment sites for the adsorption of Cu²⁺. As SA-Ch revealed the best adsorption performance, the follow-up studies were carried out on it [47].

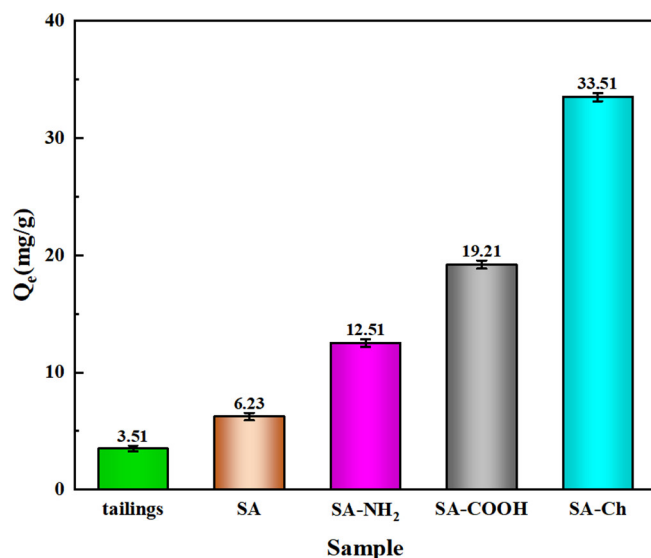


Figure 10. Adsorption capacity of Cu²⁺ by the tailings, SA, SA-NH₂, SA-COOH, and SA-Ch.

Figure 11 shows the adsorption capacity of SA-Ch at different contact times. It could be seen that within 0–2 h, the adsorption capacity increased with the extension of the

contact time. When the contact time exceeded 2 h, the adsorption process reached an equilibrium and the adsorption capacity no longer changed with the time. In the early stage of adsorption, the adsorption process mainly occurred on the surface of SA-Ch and the adsorption speed was faster because the surface was rich in hydroxyl and amino groups. With an increase in the contact time, the adsorption sites on the surface were gradually occupied by Cu^{2+} to reach saturation, the adsorption capacity almost did not grow, and the adsorption process reached an equilibrium. Thus, a contact time of 2 h was selected as the optimal contact time.

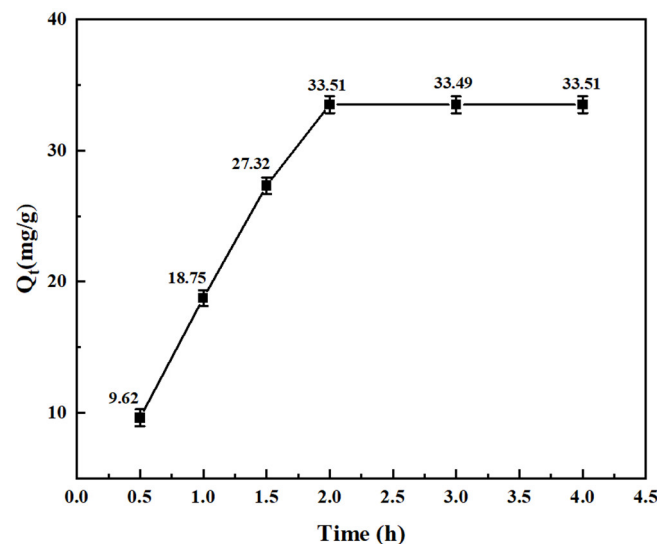


Figure 11. Effects of contact time on the adsorption of Cu^{2+} onto SA-Ch.

Figure 12 shows the adsorption capacity of SA-Ch in the solutions with different copper ion concentrations. It could be seen that when SA-Ch was in a solution with a lower copper ion concentration, the adsorption capacity of SA-Ch to the copper ions was relatively low. When the copper ion concentration increased to 100 mg/L, the adsorption capacity of SA-Ch to the copper ions reached a maximum of 33.51 mg/g. When the concentration of copper ions continued to increase, the adsorption capacity of SA-Ch stopped increasing, indicating that SA-Ch had reached an adsorption equilibrium. As a result, the optimal initial concentration was 100 mg/L.

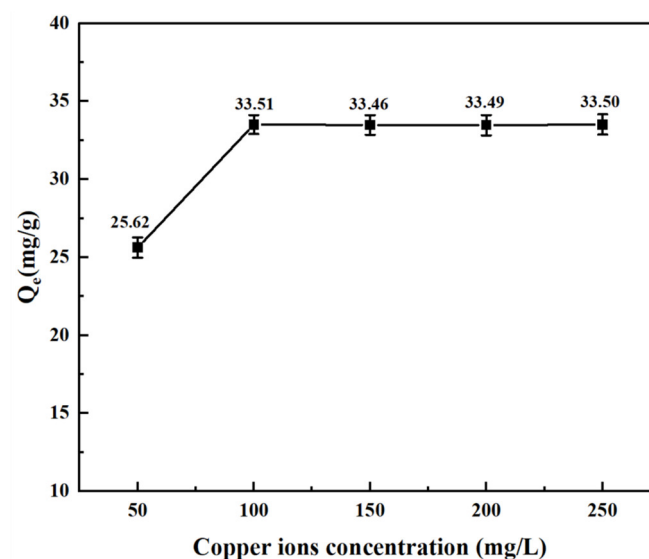


Figure 12. Effects of copper ion concentration on the adsorption of Cu^{2+} onto SA-Ch.

Figure 13 shows the adsorption capacity of SA-Ch in the copper ion solutions with different pH values. It could be seen that the adsorption capacity of SA-Ch to Cu^{2+} increased with an increase in pH. The low adsorption capacity of SA-Ch to Cu^{2+} under lower pH conditions was attributed to saturated H^+ and Cu^{2+} competing for the adsorption sites, resulting in a decreased number of adsorption centers of Cu^{2+} . In addition, the functional groups such as amino groups and hydroxyl groups showed protonation and electrostatic repulsion on Cu^{2+} also further reduced the adsorption capacity of SA-Ch on Cu^{2+} . With an increase in the pH of the solution, the competition between Cu^{2+} and H^+ was weakened due to the decrease in the H^+ concentration, resulting in more Cu^{2+} being fixed on SA-Ch. In addition, under higher pH conditions, the bound H^+ ions were gradually dissociated from the hydroxyl groups and carboxyl groups [48], which enhanced their interaction with Cu^{2+} and further increased the adsorption capacity of SA-Ch to Cu^{2+} . This showed that the adsorption of Cu^{2+} by SA-Ch was mainly due to the ion exchange and electrostatic gravity.

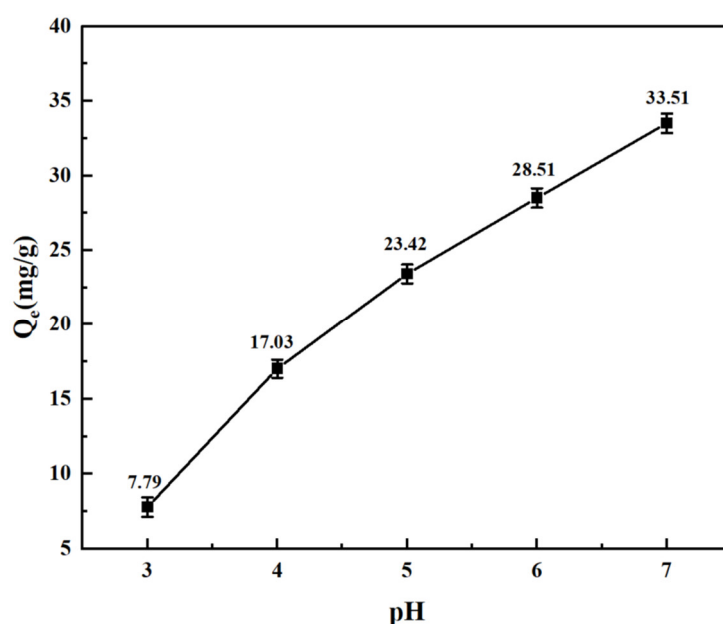


Figure 13. Effects of pH on the adsorption of Cu^{2+} onto SA-Ch.

4. Conclusions

In this work, gold tailings were used as the silicon source and a low-cost preparation of a silica aerogel was realized by combining alkali melting, the sol-gel method, and the atmospheric pressure drying method. The surface of the silica aerogel was grafted with (3-Aminopropyl) triethoxysilane (APTES), ethylenediaminetetraacetic acid disodium salt (EDTA-2Na), and chitosan to improve its adsorption performance. The results showed that the chemical composition of the prepared SA sample contained 91.1% silica and it was amorphous silica. Corresponding groups appeared on the surface of the grafted SA and the agglomeration phenomenon of the nanoparticles was obvious. The original SA and modified SAs had a large specific surface area, total pore volume, and pore diameter. The adsorption effect of the modified SAs on the copper ions was remarkable. The chitosan-modified aerogels (SA-Ch) had a better adsorption performance when using them to adsorb copper ions. SA-Ch had the highest adsorption capacity of copper ions under the conditions of an initial concentration of 100 mg/L, a pH value of 7, and an adsorption time of 2 h, which was 33.51 mg/g. The adsorption of Cu^{2+} was mainly due to the ion exchange and electrostatic gravity.

Author Contributions: Conceptualization, F.W. and Y.W.; methodology, F.W. and Y.W.; software, J.B. and K.C.; validation, F.W. and K.C.; formal analysis, F.W. and J.B.; investigation, Y.W. and K.C.; resources, F.W.; data curation, K.C. and F.W.; writing—original draft preparation, J.B., K.C., Y.W., B.F.

and F.W.; writing—review and editing, F.W. and B.F.; visualization, Y.W. and B.F.; supervision, F.W. and B.F.; project administration, F.W.; funding acquisition, F.W. All authors have read and agreed to the published version of the manuscript.

Funding: This work was financially supported by the National Key R&D Program of China (No. 2021YFC1910605), the National Natural Science Foundation of China (No. 51874115), the Introduced Overseas Scholars Program of Hebei Province, China (No. C201808), and the Excellent Young Scientist Foundation of Hebei Province, China (No. E2018202241).

Conflicts of Interest: The authors declare no conflict of interest.

References

1. Wang, X.; Wang, J.; Teng, W.; Du, Y.; Wu, J.; Guo, F.; Chen, B. Fabrication of highly efficient magnesium silicate and its adsorption behavior towards Cr(VI). *Microporous Mesoporous Mater.* **2021**, *323*, 111196. [[CrossRef](#)]
2. Sun, L.; Wu, J.; Wang, J.; Yang, Y.; Xu, M.; Liu, J.; Yang, C.; Cai, Y.; He, H.; Du, Y.; et al. In-situ constructing nanostructured magnesium ferrite on steel slag for Cr(VI) photoreduction. *J. Hazard. Mater.* **2022**, *422*, 126951. [[CrossRef](#)] [[PubMed](#)]
3. Ye, M.; Li, G.; Yan, P.; Ren, J.; Zheng, L.; Han, D.; Sun, S.; Huang, S.; Zhong, Y. Removal of metals from lead-zinc mine tailings using bioleaching and followed by sulfide precipitation. *Chemosphere* **2017**, *185*, 1189–1196. [[CrossRef](#)]
4. Stala, L.; Ulatowska, J.; Polowczyk, I. A review of polyampholytic ion scavengers for toxic metal ion removal from aqueous systems. *Water Res.* **2021**, *203*, 117523. [[CrossRef](#)]
5. Qasem, N.A.A.; Mohammed, R.H.; Lawal, D.U. Removal of heavy metal ions from wastewater: A comprehensive and critical review. *npj Clean Water* **2021**, *4*, 36. [[CrossRef](#)]
6. Liu, J.; Liu, A.; Zhang, W.-x. The influence of polyelectrolyte modification on nanoscale zero-valent iron (nZVI): Aggregation, sedimentation, and reactivity with Ni(II) in water. *Chem. Eng. J.* **2016**, *303*, 268–274. [[CrossRef](#)]
7. d’Halluin, M.; Rull-Barrull, J.; Bretel, G.; Labrugère, C.; Le Grogne, E.; Felpin, F.-X. Chemically Modified Cellulose Filter Paper for Heavy Metal Remediation in Water. *ACS Sustain. Chem. Eng.* **2017**, *5*, 1965–1973. [[CrossRef](#)]
8. Siddiqui, S.I.; Chaudhry, S.A. A review on graphene oxide and its composites preparation and their use for the removal of As³⁺ and As⁵⁺ from water under the effect of various parameters: Application of isotherm, kinetic and thermodynamics. *Process. Saf. Environ. Prot.* **2018**, *119*, 138–163. [[CrossRef](#)]
9. Feng, X.; Long, R.; Wang, L.; Liu, C.; Bai, Z.; Liu, X. A review on heavy metal ions adsorption from water by layered double hydroxide and its composites. *Sep. Purif. Technol.* **2022**, *284*, 120099. [[CrossRef](#)]
10. Xiao, Z.; Li, Z.; Meng, X.; Wang, R. MXene-engineered lithium–sulfur batteries. *J. Mater. Chem. A* **2019**, *7*, 22730–22743. [[CrossRef](#)]
11. Kolodynska, D.; Geca, M.; Skwarek, E.; Goncharuk, O. Titania-Coated Silica Alone and Modified by Sodium Alginate as Sorbents for Heavy Metal Ions. *Nanoscale Res. Lett* **2018**, *13*, 96. [[CrossRef](#)] [[PubMed](#)]
12. Gdula, K.; Dąbrowski, A.; Skwarek, E. Synthesis, surface characterization and electrokinetic properties of colloidal silica nanoparticles with magnetic core. *Adsorption* **2016**, *22*, 681–688. [[CrossRef](#)]
13. Li, J.; Dong, X.; Liu, X.; Xu, X.; Duan, W.; Park, J.; Gao, L.; Lu, Y. Comparative Study on the Adsorption Characteristics of Heavy Metal Ions by Activated Carbon and Selected Natural Adsorbents. *Sustainability* **2022**, *14*, 15579. [[CrossRef](#)]
14. Mo, L.; Zhang, S.; Qi, F.; Huang, A. Highly stable cellulose nanofiber/polyacrylamide aerogel via in-situ physical/chemical double crosslinking for highly efficient Cu(II) ions removal. *Int. J. Biol. Macromol.* **2022**, *209*, 1922–1932. [[CrossRef](#)] [[PubMed](#)]
15. Gladysz-Plaska, A.; Skwarek, E.; Budnyak, T.M.; Kolodynska, D. Metal Ions Removal Using Nano Oxide Pyrolox Material. *Nanoscale Res. Lett.* **2017**, *12*, 95. [[CrossRef](#)]
16. Mazrouei-Sebdani, Z.; Begum, H.; Schoenwald, S.; Horoshenkov, K.V.; Malfait, W.J. A review on silica aerogel-based materials for acoustic applications. *J. Non-Cryst. Solids* **2021**, *562*, 120770. [[CrossRef](#)]
17. Mazrouei-Sebdani, Z.; Naeimirad, M.; Peterek, S.; Begum, H.; Galmarini, S.; Pursche, F.; Baskin, E.; Zhao, S.; Gries, T.; Malfait, W.J. Multiple assembly strategies for silica aerogel-fiber combinations—A review. *Mater. Des.* **2022**, *223*, 111228. [[CrossRef](#)]
18. Mobley, L.R.; Scott, L.; Rutherford, Y.; Kuo, T.M. Using residential segregation to predict colorectal cancer stage at diagnosis: Two different approaches. *Ann. Epidemiol.* **2017**, *27*, 10–19. [[CrossRef](#)]
19. Zhang, X.; Chen, Z.; Zhang, J.; Yu, Q.; Cui, S. Rapid synthesis of silica aerogels by microwave irradiation. *J. Porous Mater.* **2021**, *28*, 1469–1479. [[CrossRef](#)]
20. Han, H.; Wei, W.; Jiang, Z.; Lu, J.; Zhu, J.; Xie, J. Removal of cationic dyes from aqueous solution by adsorption onto hydrophobic/hydrophilic silica aerogel. *Colloids Surf. A Physicochem. Eng. Asp.* **2016**, *509*, 539–549. [[CrossRef](#)]
21. Liu, Q.; Liu, Y.; Zhang, Z.; Wang, X.; Shen, J. Adsorption of cationic dyes from aqueous solution using hydrophilic silica aerogel via ambient pressure drying. *Chin. J. Chem. Eng.* **2020**, *28*, 2467–2473. [[CrossRef](#)]
22. Wiehn, M.; Levario, T.J.; Staggs, K.; Linneen, N.; Wang, Y.; Pfeffer, R.; Lin, Y.S.; Nielsen, D.R. Adsorption of Short-Chain Alcohols by Hydrophobic Silica Aerogels. *Ind. Eng. Chem. Res.* **2013**, *52*, 18379–18385. [[CrossRef](#)]
23. Mazrouei-Sebdani, Z.; Salimian, S.; Khoddami, A.; Shams-Ghahfarokhi, F. Sodium silicate based aerogel for absorbing oil from water: The impact of surface energy on the oil/water separation. *Mater. Res. Express* **2019**, *6*, 085059. [[CrossRef](#)]

24. Perdigoto, M.L.; Martins, R.C.; Rocha, N.; Quina, M.J.; Gando-Ferreira, L.; Patricio, R.; Duraes, L. Application of hydrophobic silica based aerogels and xerogels for removal of toxic organic compounds from aqueous solutions. *J. Colloid Interface Sci.* **2012**, *380*, 134–140. [[CrossRef](#)] [[PubMed](#)]
25. Ihsanullah, I.; Sajid, M.; Khan, S.; Bilal, M. Aerogel-based adsorbents as emerging materials for the removal of heavy metals from water: Progress, challenges, and prospects. *Sep. Purif. Technol.* **2022**, *291*, 120923. [[CrossRef](#)]
26. Pornchuti, B.; Pongpattananurak, B.; Sutthiard, D.; Singthong, P. Adsorption of copper, nickel and chromium ions using silica aerogel synthesized by ambient-pressure drying and modified with EDTA. *IOP Conf. Ser. Mater. Sci. Eng.* **2020**, *778*, 012133. [[CrossRef](#)]
27. Liu, T.; Liu, Q.; Liu, Y.; Yao, H.; Zhang, Z.; Wang, X.; Shen, J. Fabrication of methyl acrylate modified silica aerogel for capture of Cu²⁺ from aqueous solutions. *J. Sol.-Gel Sci. Technol.* **2021**, *98*, 389–400. [[CrossRef](#)]
28. Han, X.; Wang, Y.; Zhang, N.; Meng, J.; Li, Y.; Liang, J. Facile synthesis of mesoporous silica derived from iron ore tailings for efficient adsorption of methylene blue. *Colloids Surf. A Physicochem. Eng. Asp.* **2021**, *617*, 126391. [[CrossRef](#)]
29. Dong, K.; Xie, F.; Wang, W.; Chang, Y.; Lu, D.; Gu, X.; Chen, C. The detoxification and utilization of cyanide tailings: A critical review. *J. Clean. Prod.* **2021**, *302*, 126946. [[CrossRef](#)]
30. Hong, W.; Liu, X.; Srinivasakannan, C.; Duan, X.; Wang, X. Novel Aerogel Absorbent Derived from Iron Tailings Via Atmospheric Drying. *Arab. J. Sci. Eng.* **2021**, *47*, 6901–6914. [[CrossRef](#)]
31. Rodríguez-Estupiñán, P.; Legnoverde, M.S.; Simonetti, S.; Díaz Compañy, A.; Juan, A.; Giraldo, L.; Moreno-Piraján, J.C.; Basaldella, E.I. Influence of functionalization, surface area and charge distribution of SBA15-based adsorbents on CO (II) and NI (II) removal from aqueous solutions. *J. Environ. Chem. Eng.* **2020**, *8*, 103671. [[CrossRef](#)]
32. Sun, D.; Qin, Z.; Gao, J.; Gao, Y. Improvement of spectrophotometric method for determination of copper ions concentration in solution by copper reagent. *Chem. Eng.* **2019**, *33*, 70–73.
33. Jiang, Z.; Chen, K.; Zhang, Y.; Wang, Y.; Wang, F.; Zhang, G.; Dionysiou, D.D. Magnetically recoverable MgFe₂O₄/conjugated polyvinyl chloride derivative nanocomposite with higher visible-light photocatalytic activity for treating Cr(VI)-polluted water. *Sep. Purif. Technol.* **2020**, *236*, 116272. [[CrossRef](#)]
34. Ji, X.; Zhou, Q.; Qiu, G.; Yue, C.; Guo, M.; Chen, F.; Zhang, M. Preparation of monolithic silica-based aerogels with high thermal stability by ambient pressure drying. *Ceram. Int.* **2018**, *44*, 11923–11931. [[CrossRef](#)]
35. Feng, Q.; Chen, K.; Ma, D.; Lin, H.; Liu, Z.; Qin, S.; Luo, Y. Synthesis of high specific surface area silica aerogel from rice husk ash via ambient pressure drying. *Colloids Surf. A Physicochem. Eng. Asp.* **2018**, *539*, 399–406. [[CrossRef](#)]
36. Kaya Ekinçi, E.; Oktar, N. Production of value-added chemicals from esterification of waste glycerol over MCM-41 supported catalysts. *Green Process. Synth.* **2019**, *8*, 128–134. [[CrossRef](#)]
37. Tang, R.; Hong, W.; Srinivasakannan, C.; Liu, X.; Wang, X.; Duan, X. A Novel Mesoporous Fe-Silica Aerogel Composite with Phenomenal Adsorption Capacity for Malachite Green. *Sep. Purif. Technol.* **2022**, *281*, 119950. [[CrossRef](#)]
38. Hu, W.; Li, M.; Chen, W.; Zhang, N.; Li, B.; Wang, M.; Zhao, Z. Preparation of Hydro-phobic Silica Aerogel with Kaolin Dried at Ambient Pressure. *Colloids Surf. A Physicochem. Eng. Asp.* **2016**, *501*, 83–91. [[CrossRef](#)]
39. Shi, L.; Zeng, F.; Cheng, X.; Lam, K.H.; Wang, W.; Wang, A.; Jin, Z.; Wu, F.; Yang, Y. Enhanced performance of lithium-sulfur batteries with high sulfur loading utilizing ion selective MWCNT/SPANI modified separator. *Chem. Eng. J.* **2018**, *334*, 305–312. [[CrossRef](#)]
40. Sun, D.; Li, K.; Sui, X.; Zhou, C.; Liu, F. Research of silica aerogels prepared by acidic silica sol under the condition of atmospheric pressure drying. *J. Porous Mater.* **2017**, *25*, 341–349. [[CrossRef](#)]
41. Huang, J.; Ye, M.; Qu, Y.; Chu, L.; Chen, R.; He, Q.; Xu, D. Pb (II) removal from aqueous media by EDTA-modified mesoporous silica SBA-15. *J. Colloid Interface Sci.* **2012**, *385*, 137–146. [[CrossRef](#)]
42. Khedkar, M.V.; Somvanshi, S.B.; Humbe, A.V.; Jadhav, K.M. Surface modified sodium silicate based superhydrophobic silica aerogels prepared via ambient pressure drying process. *J. Non-Cryst. Solids* **2019**, *511*, 140–146. [[CrossRef](#)]
43. Zhao, W.; Fu, Y.; Chen, Y.; Sun, J.; Tang, Q.; Jiang, B.; Kong, H.; Xu, F.; Ji, Q. Effective fenton catalyst from controllable framework doping of Fe in porous silica spheres. *Microporous Mesoporous Mater.* **2021**, *312*, 110704. [[CrossRef](#)]
44. Zhang, Y.; Xiang, L.; Shen, Q.; Li, X.; Wu, T.; Zhang, J.; Nie, C. Rapid synthesis of dual-mesoporous silica aerogel with excellent adsorption capacity and ultra-low thermal conductivity. *J. Non-Cryst. Solids* **2021**, *555*, 120547. [[CrossRef](#)]
45. Zhang, L.; Zhang, H.; Guo, W.; Tian, Y. Removal of Malachite Green and Crystal Violet Cationic Dyes from Aqueous Solution Using Activated Sintering Process Red Mud. *Appl. Clay Sci.* **2014**, *93–94*, 85–93.
46. Muttakin, M.; Mitra, S.; Thu, K.; Ito, K.; Saha, B.B. Theoretical Framework to Evaluate Minimum Desorption Temperature for Iupac Classified Adsorption Isotherms. *Int. J. Heat Mass Transf.* **2018**, *122*, 795–805. [[CrossRef](#)]
47. Ebisike, K.; Okoronkwo, A.E.; Alaneme, K.K. Adsorption of Cd (II) on chitosan–silica hybrid aerogel from aqueous solution. *Environ. Technol. Innov.* **2019**, *14*, 100337. [[CrossRef](#)]
48. Vareda, J.P.; Duraes, L. Efficient adsorption of multiple heavy metals with tailored silica aerogel-like materials. *Environ. Technol.* **2019**, *40*, 529–541. [[CrossRef](#)]

Disclaimer/Publisher’s Note: The statements, opinions and data contained in all publications are solely those of the individual author(s) and contributor(s) and not of MDPI and/or the editor(s). MDPI and/or the editor(s) disclaim responsibility for any injury to people or property resulting from any ideas, methods, instructions or products referred to in the content.